J Mater Sci (2011) 46:108–116
DOI 10.1007/s10853-010-4845-1

Strength and aging behavior of Mo/Pt multilayers

A. Bellou · D. F. Bahr

Received: 19 May 2010 / Accepted: 16 August 2010 / Published online: 27 August 2010

Abstract The strength of Mo/Pt multilayers as a function of layer thickness has been investigated using nanoindentation. Structures with layer thicknesses varying from 20 to 100 nm were sputter deposited and the hardness of the films was measured using nanoindentation. It is shown that at this length scale the strengthening behavior of the films can be described by the confined layer slip model which has been proposed for other multilayered systems. Of specific interest in this study was the increase in the strength of the films after aging in ambient conditions with no apparent change in modulus. X-ray photoelectron spectroscopy revealed partial oxidation of the Mo layers in the aged samples which was associated with an increase in the residual compressive stress of the films measured by the bulge testing technique. The formation of molybdenum oxides in the Mo layer could account for the increase in strength through a second phase precipitation strengthening mechanism.

Introduction

Multilayer metallic nanocomposites have improved properties compared to their individual constituents making them attractive for a large number of applications [1, 2]. A significant amount of research has focused on their mechanical behavior since large increases in strength are observed as the layer thickness decreases from the sub micrometer to the nanometer scale [1, 3–5]. In [4], Misra and Kung have reported strength values equal to one-half or one-third of the theoretical strength for layer thicknesses of a few nanometers. The dependency of strength on layer thickness is not monotonic, implying that different strengthening mechanisms are responsible for the observed mechanical behavior at different length scales. At large layer thicknesses ($h > 100$ nm) the strengthening behavior is attributed to dislocation pile-ups at grain boundaries and interfaces in accordance to the Hall–Petch model [3, 6] with the strength of the composite being proportional to $h^{-1/2}$. As the layer thickness decreases a breakdown of the Hall–Petch regime is observed. Although the strength continues to increase as the layer thickness decreases, a dependency of h^{-a} is observed in this case, where a is different from 1/2. A single dislocation strengthening mechanism has been used to explain this behavior [3]. A plateau in strength or even softening has been observed with further decreases in layer thickness [3].

Many studies on multilayers have focused on Cu as the FCC metal [7–9] in both coherent and incoherent nanocomposite systems. In this study, the strengthening behavior of a Pt-based multilayer system is studied. Pt is an FCC metal commonly utilized in the fabrication of piezoelectric Pt/Pb(Zr_xTi_{1-x})O_3 (Pt/PZT) films [10] that can be used as MEMS acoustic transducers. The Pt/PZT film is deposited on a Si/SiO_2-etched window as a substrate; the substrate provides support and allows the membrane to withstand high pressures. Reducing the support layers and maximizing the fraction of PZT increases the acoustic performance of the device [11]. So far, attempts to make Pt free standing have not been successful.

In this study, Pt was layered with another metal to form a nanocomposite in an attempt to improve the mechanical properties of the Pt thin film. Mo, which has a BCC crystal structure, was the metal chosen as the second constituent of the multilayer film. FCC–BCC bilayer systems often

A. Bellou (✉) · D. F. Bahr
School of Mechanical and Materials Engineering,
PO Box 642920, Pullman, WA 99164-2920, USA
e-mail: abellou@wsu.edu

exhibit incoherent interfaces when the lattice misfit strain is large. An example of such a system is the Cu/Nb multilayer with a misfit strain of about 11%. In this case, no misfit dislocations are present at the interfaces between the two metallic layers [5] which are described as incoherent. However, for the Mo/Pt system, assuming a Kurdjumov–Sachs orientation with {110}Mo//{111}Pt and ⟨111⟩Mo// ⟨110⟩Pt which has been shown to be the case for other polycrystalline FCC–BCC multilayers [12–14], the lattice misfit strain is only 1.6%. In this case, the nanocomposite could exhibit misfit dislocations at the interfaces, and the system can be more accurately described as semi-coherent. The Mo/Pt multilayer was expected to show higher strength and lower net residual stress than that of the Pt film alone, since Mo thin films typically develop compressive residual stresses upon sputtering for the thicknesses used in this study [15, 16].

In order to study the strengthening behavior of the Mo/Pt multilayer system as a function of layer thickness, a number of different bilayer periods were used. The hardness and modulus of the nanocomposites were measured using nanoindentation and the residual stress of the films was determined using the bulge testing technique. The aging of the films in ambient conditions was also investigated and X-ray photoelectron spectroscopy (XPS) was used to correlate the observed mechanical behavior with the microstructure of the multilayers.

Experimental details

The nanolayered films used in this study were deposited by sequential DC magnetron sputtering at nominally room temperature onto thermally oxidized Si wafers that had been etched to form Si/SiO_2 windows approximately 2.5 μm thick. The wafers were boron doped on one side, and standard photolithography techniques were used to create the windows. Both square and rectangular geometries were fabricated with nominal lateral dimensions of 4 mm × 4 mm and 1.5 mm × 10 mm correspondingly. The thickness of the SiO_2 layer was approximately 120 nm. Mo was directly sputtered on the oxide layer for all structures. Films with 4, 10, and 20 layers were sputtered on the thermally oxidized Si wafers, which were rotated over the sputtering targets to provide film thickness and structure uniformity. The nominal thicknesses of the individual layers for each nanocomposite used in this study are shown in Table 1. The background pressure in the chamber prior to sputtering was 1×10^{-6} Torr. All Mo layers were sputtered at a regulated power of 200 W and an Ar pressure of 3.8 mTorr while the Pt layers were sputtered at a regulated power of 60 W and an Ar pressure of 11 mTorr. The use of the same sputtering conditions for all the nanostructures ensured that the deposition rates in each case were kept constant and different layer thicknesses were obtained by appropriately varying the deposition time. In addition to the Mo/Pt multilayers that were deposited on Si wafers, films with bilayer periods of 25/30 nm and 100/100 nm were also sputtered on soda lime glass slides which were used to collect X-ray diffraction patterns. The use of glass substrates ensured that only peaks originating from the films were collected. A Siemens D-500 X-ray powder diffractometer with a Cu X-ray tube was used to collect the diffraction data.

Table 1 Hardness and reduced modulus values for all multilayered Mo/Pt films used in this study

Mo/Pt film	H (GPa)	E_r (GPa)
20/20 nm (18/21 nm)	6.6 ± 0.3	128 ± 3
25/30 nm (25/29 nm)	6.3 ± 0.3	140 ± 3
60/35 nm (60/34 nm)	5.9 ± 0.5	139 ± 6
35/100 nm (33/94 nm)	3.7 ± 0.4	126 ± 7
55/100 nm (55/107 nm)	3.8 ± 0.5	131 ± 7
100/100 nm (93/102 nm)	4.3 ± 0.3	125 ± 4
Mo film (500 nm)	5.9 ± 0.6 (~50 nm contact depth)	131 ± 7
Pt film (500 nm)	1.5 ± 0.2 (~80 nm contact depth due to large surface roughness)	100 ± 8

The top view and cross sections of the nanocomposites, which were acquired by cleavage, were examined using a FEI Sirion 200 Scanning Electron Microscope (SEM). The actual layer thicknesses of the multilayers were measured from the SEM micrographs and are also presented in Table 1 along with the nominal thicknesses.

The modulus and hardness of the films were measured using a Hysitron Triboscope with the nanoDMA™ attachment which records the contact stiffness at various points during loading, allowing modulus and hardness to be measured as a function of penetration depth for a given indentation. A calibrated Berkovich tip was used for the indentations. All hardness values reported here refer to values measured at contact depths that correspond to approximately 10% of the total film thickness. This choice minimizes the influence from the substrate on the reported values and at the same time is deep enough to minimize any effects from surface roughness. Each sample was indented at least five times, and 80 measurements per indent were collected. The values of hardness and reduced modulus presented in Table 1 are averages of the indentations at the aforementioned contact depth.

A bulge testing apparatus was used to measure the modulus and residual stress of the films that were fabricated into membranes. A Polytec OFV 511 scanning laser vibrometer recorded the displacement of the center of the

membrane as a function of pressure. The pressure was applied using a Meriam Pressure/Vacuum variator [11].

X-ray photoelectron spectroscopy spectra were also collected for the 100/100 nm and 25/30 nm Mo/Pt films with an AXIS-165 manufactured by Kratos Analytical, Inc. An achromatic Mg Kα (1254 eV) X-ray radiation was used with a power of 210 W. The spectrometer was calibrated using the Au $4f_{7/2}$ peak at 84.2 eV and the Ag $3d_{5/2}$ peak at 368.5 eV. In order to investigate the chemistry of the nanolayered films, depth profiles were collected. The first two layers of each nanostructure were probed by using Ar^+ sputtering at 4 keV and collecting XPS spectra at regular sputtering time intervals. Mo and Pt films, deposited at the same sputtering conditions as the individual layers of the nanocomposite, were used as reference samples for the XPS analysis.

Results and discussion

Strength enhancements with decreasing layer thickness

As shown in Fig. 1, a top view of the as grown films, the in plane grain size is small, ranging from 10 to 30 nm, with somewhat faceted grains. Some voiding along the grain boundaries is also observed, indicative of Zone I film growth [17]. These characteristics are common for all films used in this study irrespective of layer thickness. Typical cross sections, acquired using cleavage, are presented in Fig. 2. The columnar structure of the Pt grains can be clearly seen for the structure with the thicker layers.

The hardness and reduced modulus as a function of contact depth for all films were determined using nanoindentation. Measurements for both as deposited films and films aged in ambient conditions for 3 months were collected, and the hardness and reduced modulus for the aged films at approximately 10% of the total film thickness are reported in Table 1 and presented in Figs. 3 and 4 correspondingly. In the same table, the hardness and reduced modulus for the reference Mo and Pt films with a thickness of 500 nm are also reported. We choose to report the values for reduced modulus as these are directly measured from the nanoindentation experiment. In this case, the diamond tip is much stiffer than the films, so the values for reduced and Young's modulus are essentially the same. For example, in the case of the nominally 100/100 nm Mo/Pt film if we assume that $\nu = 0.07$ and $E = 1141$ GPa for the diamond tip and use a weighted average of $\nu = 0.35$ for the Poisson's ratio of the film, the Young's modulus is found equal to 123 GPa instead of the reduced modulus value of 125 GPa.

The moduli for the as deposited Mo/Pt films are considerably lower than what would be expected from a simple rule of mixtures from their bulk constituents. However, the fact that the moduli values for the Mo and Pt films are also considerably lower than their bulk counterparts indicates that this behavior is not a result of the multilayered structure but rather of the specific thin film system. Modulus

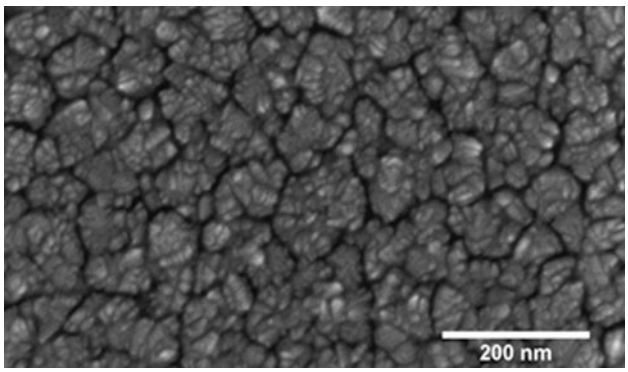

Fig. 1 Typical top view of the as deposited Mo/Pt films as seen in the SEM. The grains appear faceted and some voiding along the grain boundaries is present

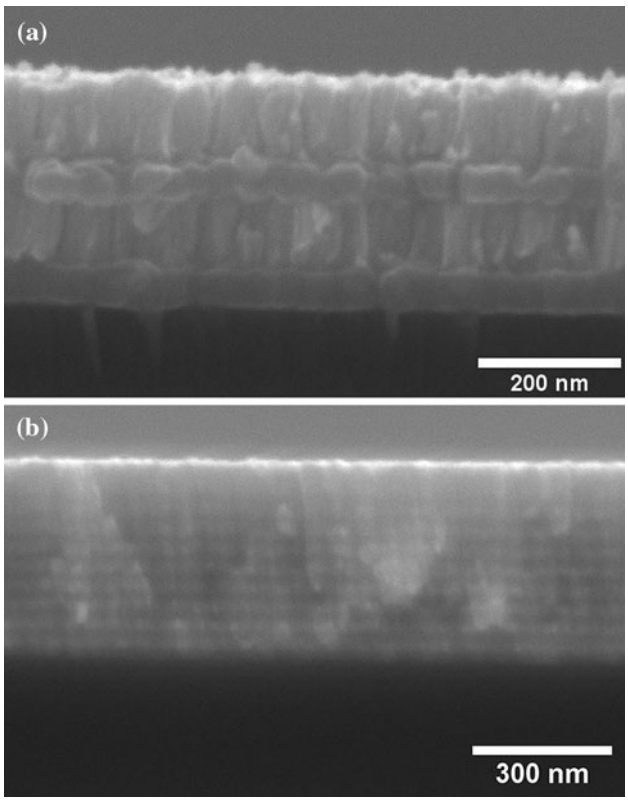

Fig. 2 Typical cross sections for a four layer (**a**) and a 20 layer (**b**) Mo/Pt nanocomposite as seen in the SEM. For the four-layered structure, the average thickness of the Mo layers is 55 nm and that of the Pt layers is 107 nm for an average total film thickness of approximately 325 nm. For the 20 layered structure, the average thicknesses for the Mo and Pt layers are 18 and 21 nm correspondingly for a total thickness of approximately 400 nm

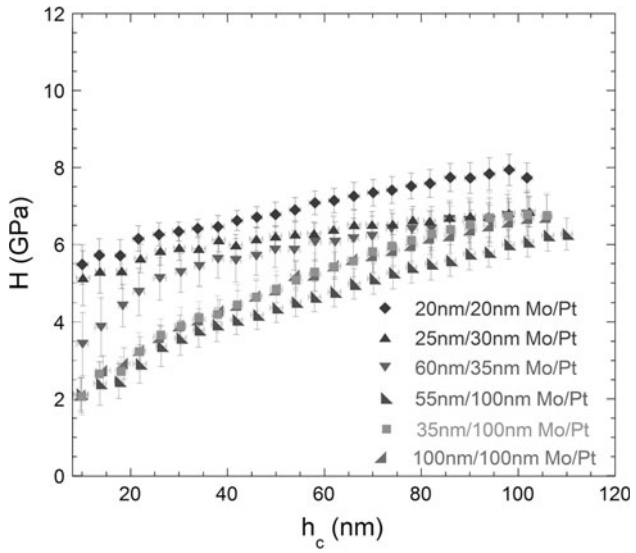

Fig. 3 Hardness as a function of contact depth for all the aged multilayers used in this study. The smaller the thickness of the Pt layer the harder the films appear

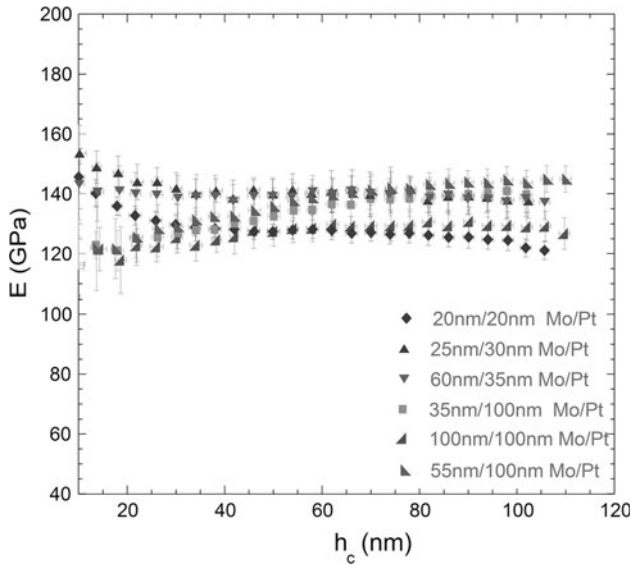

Fig. 4 Reduced modulus of all the aged multilayers as a function of contact depth

values for Mo thin films that are lower than the bulk value have been reported in literature before [18]. In [9], Spaepen and co-workers found lower modulus values for free standing FCC films and attributed this behavior to the high-grain boundary area which can provide a possible source for defects thus lowering the elastic properties of the film. In [19], the density of Mo films was correlated to the Ar pressure, and it was shown that higher Ar pressures result in lower film densities, voided grain boundaries and oxygen incorporation. The formation of oxides along the grain boundaries could account for the decrease in the elastic modulus of the Mo thin films when compared to that of the bulk material. The slightly voided grain boundaries of the Pt film could act as fast diffusion paths for oxygen which could subsequently form Mo oxides impacting the elastic properties of the nanocomposites.

The low modulus values for the multilayers and the Mo reference film were confirmed using the bulge testing technique. Pressure deflection data for the 500 nm Mo film and the 100/100 nm Mo/Pt multilayer deposited on 2.5 μm Si/SiO_2 square windows were collected. The biaxial modulus of the membranes (film and Si/SiO_2 backing substrate) was determined by curve fitting the pressure deflection data [20, 21]. The Young's modulus was calculated from the biaxial modulus using the Poisson's ratio of the membrane which was assumed to be the thickness weighted average of the corresponding ratios of the individual layers. Poisson's ratios of 0.17, 0.22 [22], 0.31, and 0.38 were used for the SiO_2, Si, Mo, and Pt layers, respectively. Finally, the Young's modulus of the metallic films alone was calculated using

$$E_{\text{tot}} = \frac{t_{\text{subs}}}{t_{\text{tot}}} \cdot E_{\text{subs}} + \frac{t_{\text{film}}}{t_{\text{tot}}} \cdot E_{\text{film}}, \quad (1)$$

where t_{subs}, t_{film}, t_{tot} are the thicknesses of the substrate, the film, and the membrane and E_{subs}, E_{film}, E_{tot} are the corresponding values of the Young's modulus.

The moduli measured using nanoindentation and those determined using the bulge testing technique for the two films (Table 2) are statistically similar, indicating that the low values are a true property of this particular structure and system. The small variation in the elastic modulus of the multilayer as determined using both methods is the result of small differences in the thickness of the Mo layer.

As shown in Table 1, the hardness values are similar when the thickness of the Pt layers is kept constant at approximately 100 nm, despite the different Mo layer thickness. The Wilcoxon Rank Sum test [23] was used to analyze the three datasets. This test compares the unpaired data of two different datasets and assigns a probability value. If this value is less than a reference value, typically 0.05, it indicates that the two populations are statistically different. The analysis for the 35/100 nm and 55/100 nm films gave a probability value higher than 0.05 indicating that differences in the average hardness values were

Table 2 Comparison of Young's modulus measured with nanoindentation and bulge testing

Film	E (GPa), nanoindentation	E (GPa), bulge testing
Mo (500 nm)	131 ± 7	144 ± 9 ($\nu = 0.23$)
Mo/Pt 100/100 nm	125 ± 4 (true layer thickness 93/102 nm)	134 ± 12 ($\nu = 0.24$) (true layer thickness 110/100 nm)

statistically insignificant. However, the differences in the hardness values of these two films when compared to the hardness of the 100/100 nm film were statistically significant despite the fact that the observed difference is small. At this length scale the Hall–Petch model, where continuum dislocation pile-ups at grain boundaries or interfaces account for increases in strength, starts to break down and other strengthening mechanisms are operating [3, 24]. Discrete dislocation pile-ups have been used to explain the strengthening behavior of the multilayers in this length scale [24] with grain boundaries and interfaces acting as obstacles to dislocation motion within the soft layer. The strength enhancement depends on the distance between these obstacles, essentially, grain size and layer thickness, which are the same for all films with a Pt thickness of 100 nm. The similarities between the hardness values of the three films, with approximately the same Pt but different Mo thicknesses, emphasizes the importance of the soft layer in the overall mechanical behavior of the film, assuming to a first approximation that no change of the interfacial structure occurs with varying thickness.

The hardness data presented in Table 1 were converted to an estimated flow stress by dividing by 2.7 [25] and plotted as a function of the Pt layer thickness (Fig. 5). The bilayer periods used in this study correspond to lengths where the confined slip of dislocations (confined layer slip, CLS model) has been used to describe the strengthening behavior of other multilayer systems [3, 5], with 100 nm being the upper limit of the length scale where this model can be applied to fit experimental data. For multilayers

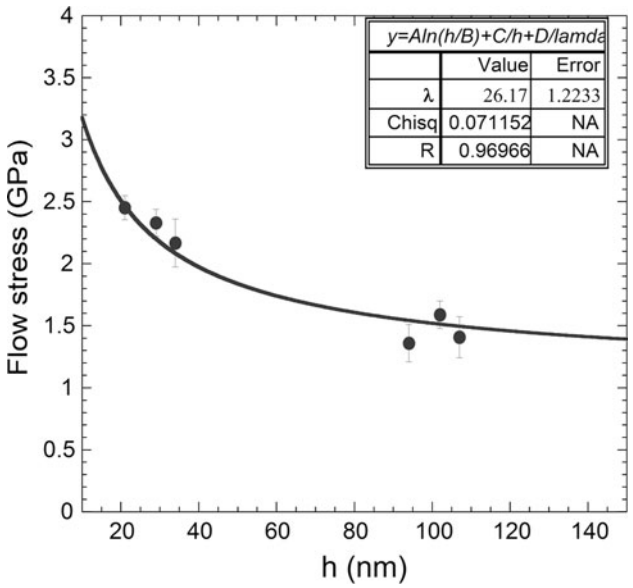

Fig. 5 Fitting of the strength data for the Mo/Pt system using the modified CLS model [5]

with incoherent interfaces, the strength of the composite as a function of layer thickness is given by [5]

$$\sigma_{\mathrm{cls}} = M\frac{\mu b}{8\pi h'}\left(\frac{4-\nu}{1-\nu}\right)\left[\ln\frac{\alpha h'}{b}\right] - \frac{f}{h} + \frac{C}{\lambda}, \qquad (2)$$

where M is the Taylor factor, μ is the shear modulus, b is the Burgers vector of the glide dislocation, h' is the layer thickness h projected on the glide plane, ν is the Poisson's ratio, α represents the core cut-off parameter, f is the interface stress, C is equal to $\mu b/(1-\nu)$, and λ is the equilibrium spacing of the misfit dislocation arrays at the interface. The first term of the equation corresponds to the stress necessary to initiate dislocation glide in a layer of thickness h whereas the second term accounts for the stress present at the interface due to elastic deformation. The third term describes the stress opposing the glide of dislocation loops from dislocation arrays already present at the interface. In [5], where this model was successfully used to fit the available strength versus layer thickness experimental data for the Cu/Nb system, the large misfit strain excludes the presence of pre-existing misfit dislocations at the interface, i.e., an incoherent interface. In the cases of Mo/Pt films, which likely have semi-coherent interfaces, and Cu/Nb with incoherent interfaces, dislocation content builds up at the interfaces as the gliding dislocation loops encounter the interfaces and are confined to move parallel to them. The stress field of these arrays will oppose the glide of new dislocations in subsequent CLS events. For the Mo/Pt system studied here, the lattice misfit strain is relatively small hence misfit dislocations can be present at the FCC–BCC interface opposing dislocation motion prior to plastic flow in addition to dislocation segments which are deposited as the confined loops glide parallel to the interface. For both types of FCC–BCC interfaces, the third term in (2) accounts for the interaction of glide dislocations on the slip planes with dislocation arrays present at the interface which can be misfit dislocations and/or dislocations deposited during previous CLS events. Equation 2 was used here to curve fit the data for the Mo/Pt system shown in Fig. 5. Values of $\mu = 61$ GPa, $b = 0.28$ nm, and $\nu = 0.38$ corresponding to Pt were used in (2). A value of 3.1 was assumed for the Taylor factor and f was set equal to 2 J/m^2, a typical value for interfacial energies [5], since this value was not available from atomistic simulations for the Mo/Pt system. The core cut-off parameter α was set equal to 0.2; a value that has been used for the Cu/Nb incoherent system [5]. The equilibrium spacing of the dislocation arrays at the Mo/Pt interface, λ, used as a fitting parameter, was found equal to 26 nm. Equating the spacing λ to b/ε, where b is the Burgers vector of the interfacial dislocations, and ε is the plastic strain and using a value of 0.28 nm for b (corresponding to a $1/2\langle 110\rangle$ dislocation in Pt) a strain of 1.1% is found. This value is

reasonable when compared to the lattice misfit strain of 1.6% calculated using the Mo and Pt lattice parameters.

Aging of multilayered films

In order to evaluate the effect of aging in ambient conditions on the mechanical properties of the films, measurements were first collected soon after film deposition and then repeated after 3 months. Comparison of the hardness values for the as deposited and aged films indicated that the hardness of the nanocomposites increased over time whereas no change in the modulus of the same films occurred. In Table 3, the hardness for as the deposited and aged films with the smaller thicknesses used in this study are presented and the increase in hardness is apparent. The values reported in this table are again averages of a large number of indents corresponding to approximately 10% of the total film thickness. Statistical analysis showed that the differences in the hardness values between the two datasets corresponding to the same layer thickness are statistically significant, with a p value of less than 0.05. A typical graph that shows the increase in strength with aging time is shown in Fig. 6 for one of the multilayers presented in Table 3 along with the corresponding modulus data.

Micrographs taken from the top and the cross sections of the aged samples revealed no significant changes in microstructure that could account for the apparent change in strength. XPS was used to examine the composition and chemical bonding of the aged samples.

Depth profiling of the aged 100/100 nm and 25/30 nm Mo/Pt films using XPS indicated the presence of Mo oxides in the Mo layer. The samples were Ar^{+} sputtered for predetermined amounts of time, and XPS spectra were collected at the end of each sputtering cycle. The depth profile for the two top layers of the four layer structure is presented in Fig. 7. In addition to Mo and Pt, O was also detected in the film and its concentration tracked with the concentration of Mo. Peak deconvolution of the Mo 3d spectra collected from well within the Mo layer indicated that in addition to elemental Mo^{0}, at a binding energy of 228.1 eV, a weak peak at 229.4 eV was also present [26]. This peak was associated to Mo^{+4} species due to the formation of MoO_2. MoO_2 was also found in the reference aged Mo film. Similar results were obtained from depth profiling the first two layers of the 25/30 nm Mo/Pt

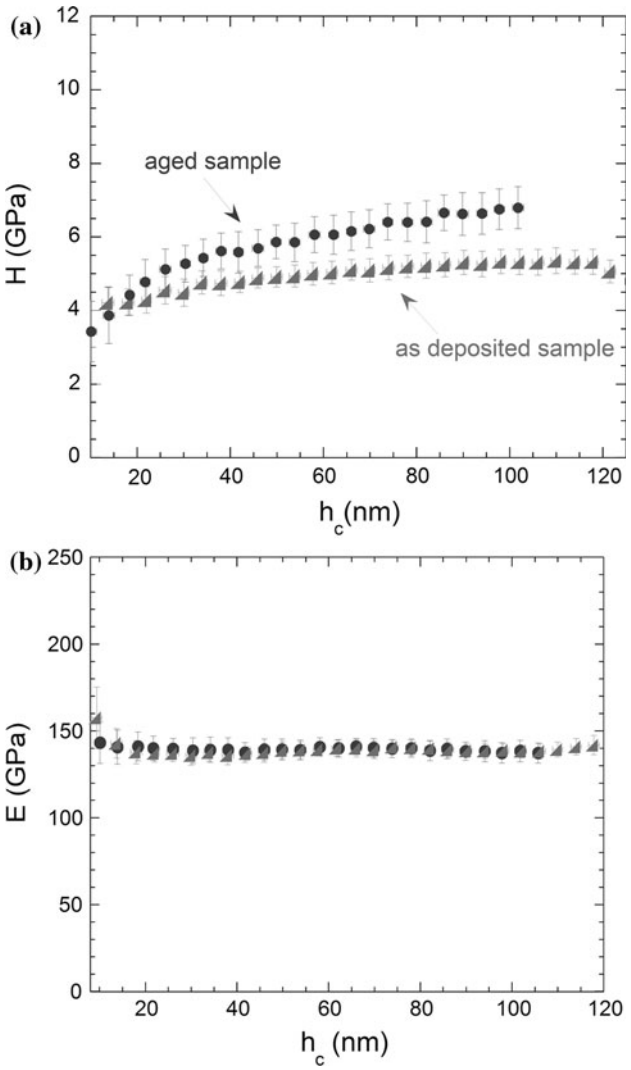

Fig. 6 Despite the observed increase in hardness for the 60/35 nm film after aging in ambient conditions for 3 months (**a**) no change in the modulus was observed (**b**)

nanocomposite. These results indicate oxygen incorporation in the multilayer structure, possibly along the Pt voided grain boundaries, and the formation of Mo oxides both at the interface between Pt and Mo as well as deep within the Mo layer.

The oxidation of Mo can occur in the deposition chamber during sputtering or by post-deposition exposure of the films in air. In [19], the presence of O in sputtered

Table 3 Comparison of hardness values for initial and aged samples (both as deposited and annealed multilayers are considered)

Multilayer	H (GPa) of as deposited films	H (GPa), after aging, of as deposited films	H (GPa) of annealed films	H (GPa), after aging, of annealed films
20/20 nm (18/21 nm)	6.1 ± 0.3	6.6 ± 0.3	–	–
25/30 nm (25/29 nm)	5.4 ± 0.3	6.3 ± 0.3	4.0 ± 0.8	3.7 ± 0.8
60/35 nm (60/34 nm)	4.9 ± 0.3	5.9 ± 0.5	4.1 ± 0.5	4.4 ± 0.7

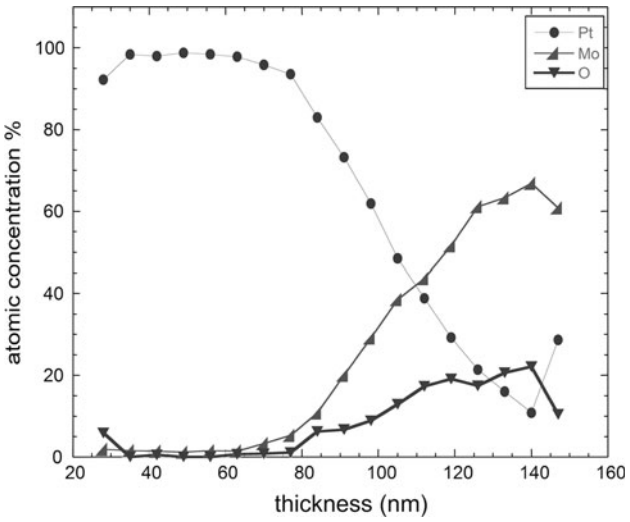

Fig. 7 Depth profiling of the 100/100 nm Mo/Pt film. The presence of O is detected in the multilayer and its concentration tracks with that of Mo

Mo films was attributed to post-deposition oxidation with higher oxygen content appearing in less dense structures, with the Ar pressure during sputtering controlling the density of the films. Oxygen incorporation in Mo causes lattice expansion and can make the stress of the film more compressive [15, 19]. Exposure of tungsten films to air at ambient temperature [27] has shown that for porous (zone I) films oxygen incorporation at the voids is possible, causing the films to become more compressive with time. The authors did not observe a similar stress evolution when the films were kept under vacuum. These studies indicate that post-deposition introduction of oxygen in thin films and more specifically in Mo films is possible. For the composites discussed here Mo is not in direct contact with air, however, the columnar structure of the Pt layers combined with the slightly voided grain boundaries could facilitate oxygen diffusion at relatively low temperatures.

Since oxygen incorporation in Mo films has been associated with stress changes, more specifically an increase in compressive stress, one would expect the residual stress of the Mo layers to change with aging time if the oxygen content increases upon exposure to ambient conditions. This change of stress in the Mo layers would not affect the stress in the Pt layers although the net stress of the nanocomposite would change. This correlation between the oxygen present in the Mo film and the changes in residual stress offers an indirect way to verify that post-deposition oxidation of the Mo layers does indeed occur.

Changes in the residual stress of thin films with an increase in the oxygen content have been reported in literature for other material systems [28, 29]. In [28], the oxidation of TiN thin films at room temperature was studied and the increase of the compressive stress in the films with time was correlated to the different stages of the oxidation process and the increase of the O content in the films. A similar evolution of the compressive stress after exposure in air was reported for Ta films in [29].

In order to check whether any changes in the net residual stress, associated with changes in the O content of Mo, occur with aging, both Mo and Mo/Pt films with two different bilayer periods were sputtered on Si/SiO_2 windows approximately 2.5 μm thick. The mechanical properties of these membranes were monitored using the bulge testing technique over time. Pressure deflection curves were recorded, and fitting parameters from these curves were used to calculate the modulus and residual stress of the films [20, 21].

The Mo films were first tested as soon as they were removed from the sputtering chamber. The elastic modulus was measured equal to 144 ± 9 GPa, and the residual stress of the structure was 19.5 ± 1.1 MPa. The membranes were left in ambient conditions and although no buckling was present on the day of sputtering, buckles appeared on the film surface on the second day. The buckling of the films prevented further measurements of the residual stress; however, it indicated an increase in the compressive stress of the films consistent with an increase in oxygen content. X-ray diffraction data collected on days 1 and 20 after sputtering did not detect a phase change in the films and only Mo peaks were present in both patterns. However, given the higher sensitivity of the XPS technique [30, 31] which has detected the presence of MoO_2 in the Mo films, the XRD results point to the very small dimensions of the forming oxides. The observed increase in the compressive stress combined with the presence of oxides in the aged Mo film supports the assumption that post-deposition formation of nanoscale oxides can be responsible for the changes in residual stress.

After verifying that a change in the residual stress of the Mo films indeed occurs upon exposure in air, the stress evolution for the Mo/Pt nanocomposites was investigated. Two different bilayer periods were chosen for monitoring stress evolution over time using bulge testing; namely, the 25/30 nm and the 100/100 nm films. Both square and rectangular window geometries were used. In the case of the 25/30 nm Mo/Pt films, all membranes, both square and rectangular, buckled immediately after deposition hence no further testing was possible.

The 100/100 nm Mo/Pt films did not buckle, allowing us to study the evolution of mechanical properties with aging in ambient conditions. In Fig. 8, the evolution of the net residual stress of the film with time is presented. The residual stress in the structure became more compressive after sputtering, with the highest change occurring within the first 24 h. The difference between the values for the

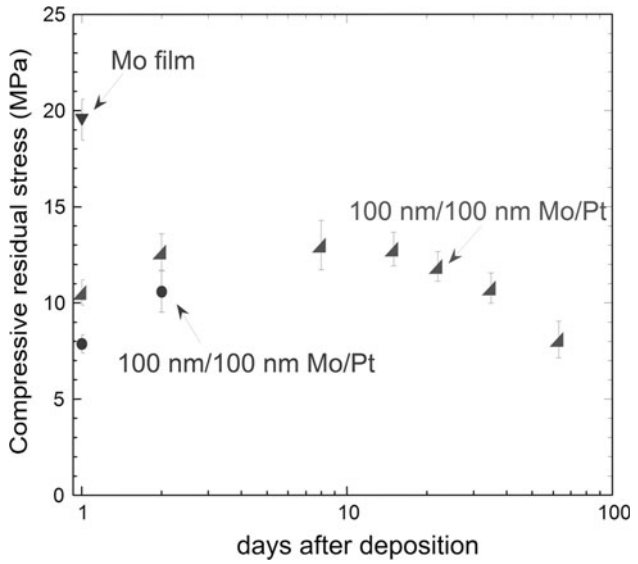

Fig. 8 Evolution of the residual stress for the 100/100 nm Mo/Pt film (two samples were used). The stress of the Mo film directly after sputtering (day 1) is also shown in this graph for comparison

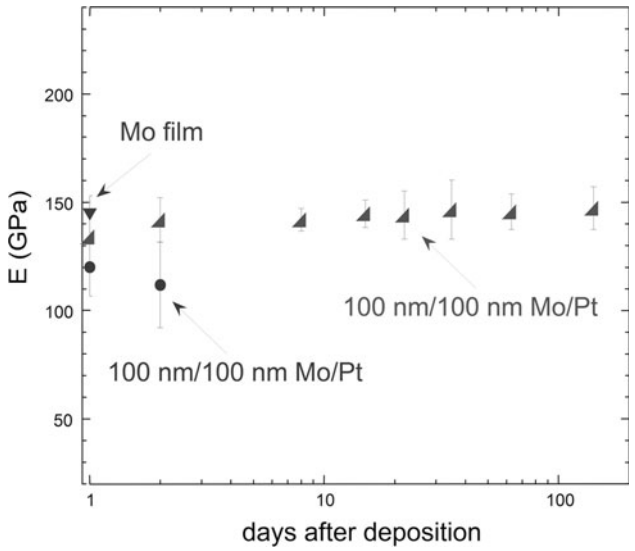

Fig. 9 Evolution of the elastic modulus of the 100/100 nm Mo/Pt film with time (two samples were used). The modulus of the Mo film is also shown here for comparison. No change was detected over time

first and second day is statistically significant, with a p probability of less than 0.05. As more days elapsed a plateau in residual stress was observed. This change in residual stress where a rapid increase is followed by a plateau in stress values indicates that the amount of oxygen incorporated in the films is a diffusion controlled process. The oxygen content would increase rapidly upon initial exposure of the film in air before reaching a plateau for longer times. After 15 days, a partial relaxation of the residual stress was observed. This relaxation with time has not been reported for other thin film systems where an increase in residual stress was attributed to O incorporation [28, 29]. The difference between those systems and the one studied here is the presence of interfaces with a large surface area compared to the volume of the nanostructure. These interfaces probably play a role in the partial relaxation of the residual stress which could involve local rearrangement along the interface boundaries to accommodate some of the stress. It is known that FCC–BCC interfaces can act as sinks for point defects [32]. It is possible that under the compressive stress present in the Mo layers O interstitials from the layer interior diffuse to the interfaces and some of the stress caused by the lattice expansion of Mo relaxes. Despite the change in the residual stress, no change was observed for the elastic modulus of the films (Fig. 9); in agreement with the nanoindentation results. This implies that the residual stress and oxidation effects on plasticity in the films are likely coupled, and at the current time, we are not able to separate these effects. Future work storing films in non-oxidizing environments will be used in an attempt to isolate these effects.

X-ray diffraction patterns collected from the Mo/Pt films over a period of time following sputtering and exposure in air, did not capture the formation of Mo oxides which has been verified by the more sensitive XPS technique [30, 31] (Fig. 7), pointing again to the small dimensions of the forming oxide.

The presence of compressive residual stresses makes the creation of free standing membranes challenging. Removal of the 2.5 μm Si/SiO_2 backing substrate caused buckling and destruction of the free standing film. Therefore, despite the small values of the compressive residual stress and the high strength achieved by substituting Pt with a Pt-based nanocomposite, this replacement leads to elastic buckling of the free standing membrane for sub-μm thicknesses.

The measurements of residual stress using bulge testing indirectly confirm the assumption that the oxygen content of the Mo/Pt films, and more specifically that of the Mo layers, changes with time when the films are exposed to air in ambient temperature. No other change in microstructure was detected and oxygen incorporation could account for the changes in residual stress with no apparent change in modulus. Post sputtering oxidation could also account for the increase in hardness with aging considering the small dimensions of the forming oxides which is implied by combining the XPS and XRD data on these films. The fine dispersion of oxides could act as additional obstacles to dislocation motion increasing the hardness of the films. This assumption is supported by the fact that the aging of Mo/Pt multilayers at ambient conditions for 3 months after they were first annealed at 475°C yielded no changes in strength. In this case, complete oxidation of all the Mo layers occurred upon annealing [26] which indicates that

the increase in hardness is related to the gradual oxidation of the Mo layers with aging time. Values for the hardness of annealed samples initially and after they were aged for 3 months are presented in Table 3. Statistical analysis showed that small variations between the hardness values for annealed and annealed films after aging of the same layer thickness were statistically insignificant.

For the Pt-based multilayers studied here, Pt is the soft layer where plastic deformation initially occurs with the slip of glide dislocations confined by the presence of the Mo/Pt interface. The increase in strength after aging in ambient conditions can be explained by the presence of Mo oxides at the Mo/Pt interface which has been captured by the XPS depth profiling. The precipitates at the interface can act as additional obstacles to dislocation motion and inhibit dislocation transmission across the interface, in the manner described by the Orowan type strengthening mechanism. In this case, the third term in Eq. 2 is more general and describes the effect that both dislocation arrays and precipitates, present at the interface, have on dislocation glide within the soft layer. It represents the stress that opposes dislocation motion from obstacles that are present at the interface, with λ being the separation distance of these obstacles.

Summary

The mechanical properties of the Mo/Pt multilayered system were studied using two techniques, nanoindentation and bulge testing. Multilayers with different bilayer periods were studied, and the hardening behavior was similar to that reported for other FCC–BCC systems. For the thickness range used in this study, the CLS model can describe the strengthening behavior of the nanocomposites. An increase in the hardness of the multilayer films after aging in ambient conditions was also observed. The combination of the results of XPS with the evolution of residual stresses in the nanolayered films after exposure to air in ambient temperature, pointed to O incorporation as responsible for the aging behavior. Oxide formation causes increases in both the strength and the compressive residual stress of the nanostructures. The increase in strength can be attributed to the formation of Mo oxides at the Mo/Pt interface which can act as obstacles to dislocation glide, in the manner described by the Orowan strengthening mechanism. Such an increase in strength was not observed with the aging of annealed Mo/Pt films at ambient conditions. In this case, complete oxidation of all the Mo layers occurred upon annealing, further confirming the assumption that post sputtering partial oxidation of the as deposited films can account for the increased strength.

Acknowledgements This study was supported in part by the US Department of Energy under Grant number DE-FG02-07ER4635. The help of Dr Louis Scudiero with the XPS analysis is also gratefully acknowledged.

References

1. Was GS, Foecke T (1996) Thin Solid Films 286:1
2. Clemens BM, Kung H, Barnett SA (1999) MRS Bull 24:20
3. Misra A, Hirth JP, Kung H (2002) Philos Mag A 82:2935
4. Misra A, Kung H (2001) Adv Eng Mater 3:217
5. Misra A, Hirth JP, Hoagland RG (2005) Acta Mater 53:4817
6. Zhang X, Misra A, Wang H, Shen TD, Nastasi M, Mitchell TE, Hirth JP, Hoagland RG, Embury JD (2004) Acta Mater 52:995
7. Misra A, Verdier M, Lu YC, Kung H, Mitchell TE, Nastasi M, Embury JD (1998) Scr Mater 39:555
8. McKeown J, Misra A, Kung H, Hoagland RG, Nastasi M (2002) Scr Mater 46:593
9. Huang H, Spaepen F (2000) Acta Mater 48:3261
10. Eakins LMR, Olson BW, Richards CD, Richards RF, Bahr DF (2003) Thin Solid Films 441:180
11. Morris DJ, Bahr DF, Anderson MJ (2008) Sens Actuators A 141:262
12. Misra A, Hirth JP, Hoagland RG, Embury JD, Kung H (2004) Acta Mater 52:2387
13. Mitchell TE, Lu YC, Griffin AJ Jr, Nastasi M, Kung H (1997) J Am Ceram Soc 80:1673
14. Fu EG, Li N, Misra A, Hoagland RG, Wang H, Zhang X (2008) Mater Sci Eng A 493:283
15. Kendig LP, Rek UZU, Yalisove SM, Bilello JC (2000) Surf Coat Technol 132:124
16. Hoffman DW, Thornton JA (1980) J Vac Sci Technol 17:380
17. Thornton JA (1977) Ann Rev Mater Sci 7:239
18. Wang J, Li W-Z, Li H-D, Shi B, Luo J-B (2000) Thin Solid Films 366:117
19. Klabunde F, Lohmann M, Blasing J, Drusedau T (1996) J Appl Phys 80:6266
20. Bonnotte E, Delobelle P, Bornier L, Trolard B, Tribillon G (1997) J Mater Res 12:2234
21. Vlassak JJ, Nix WD (1992) J Mater Res 7:3242
22. Dolbow J, Gosz M (1996) Mech Mater 23:311
23. Mann HB, Whitney DR (1947) Ann Math Stat 18(1):50
24. Anderson PM, Foecke T, Hazzledine PM (1999) MRS Bull 24:27
25. Tabor D (1951) The hardness of metals. Oxford University Press, New York
26. Bellou A, Scudiero L, Bahr DF (2010) J Mater Sci 45:354. doi: 10.1007/s10853-009-3943-4
27. Haghiri-Gosnet AM, Ladan FR, Mayeux C, Launois H, Joncour MC (1989) J Vac Sci Technol A 7(4):2663
28. Logothetidis S, Meletis EI, Stergioudis G, Adjaottor AA (1999) Thin Solid Films 338:304
29. Yoshihara T, Suzuki K (1993) J Vac Sci Technol B 11:301
30. Shen Y, Xiong T, Du H, Jin H, Shang J, Yang K (2009) J Sol-Gel Sci Technol 50:98
31. Lin X, Zhou R, Zhang J, Fei S (2009) Appl Surf Sci 256:889
32. Misra A, Demkowicz MJ, Zhang X, Hoagland RG (2007) JOM 59:62